2024-01-2790 Published 09 Apr 2024

Machine Learning Approach for Open Circuit Fault Detection and Localization in EV Motor Drive Systems

Ali Arsalan, Behnaz Papari, S M Imrat Rahman, Laxman Timilsina, Ali Moghassemi, Grace Muriithi, Gokhan Ozkan, Christopher Edrington, and Elutunji Buraimoh Clemson University

Citation: Arsalan, A., Papari, B., Rahman, S.M., Timilsina, L. et al., "Machine Learning Approach for Open Circuit Fault Detection and Localization in EV Motor Drive Systems," SAE Technical Paper 2024-01-2790, 2024, doi:10.4271/2024-01-2790.

Received: 22 Oct 2023 Revised: 08 Jan 2024 Accepted: 16 Jan 2024

Abstract

Semiconductor devices in electric vehicle (EV) motor drive systems are considered the most fragile components with a high occurrence rate for open circuit fault (OCF). Various signal-based and model-based methods with explicit mathematical models have been previously published for OCF diagnosis. However, this proposed work presents a model-free machine learning (ML) approach for a single-switch OCF detection and localization (DaL) for a two-level, three-phase inverter. Compared to already available ML models with complex feature extraction methods in the literature, a new and simple way to extract OCF feature data with sufficient classification accuracy is proposed. In this regard, the inherent property of active thermal management (ATM) based model predictive control (MPC) to quantify the conduction losses for each semiconductor device in a power converter is integrated with an ML network. This recurrent neural network (RNN)-based ML model as a multiclass classifier localizes the faulty switch based on the dynamics associated with conduction losses as reliable and feature-rich data. The presented approach utilizes the controller data with no additional computational load to compute the feed-in data for the ML model and no extra hardware requirements. The proposed data-driven approach, with an accuracy of 99% for distinct hyperparameters and testing datasets, proves to be a promising solution for OCF DaL.

Introduction

The recent advancements towards electric drive systems (EDS) have increased the utilization of inverter-fed interior permanent magnet synchronous motor (IPMSM) applications with the latest control topologies in the transportation sector [1, 2]. This EDS is considered to be one of the most important safety-critical subsystems in an EV infrastructure. Although these power electronics-based systems have evolved exponentially with the latest research progress, they are still prone to critical faults when exposed to high stress. Based on the recent statistical data, semiconductor power devices account for 31% as the most fragile component in a power converter. The most common failure modes in these semiconductor devices are open-circuit and short-circuit faults, which occur due to various reasons such as thermal stress, high *dv/dt*, and over-voltage. In the case of a short circuit fault, the power converter experiences an instant current upsurge, which triggers the protection circuit to cut off the gate-drive signal. In comparison, the OCF doesn't necessarily shut down the system immediately; instead, it can persist while causing performance degradation in the form of torque and current ripples and leads to faults in other system components. In addition, open circuit fault (OCF) accounts for 38% of the total faults that may occur in a power converter [3]. Therefore, it is important to have a viable device-level control approach that can detect and localize an OCF before its effects propagate to other subsystems.

An OCF in a power switch causes characteristic distortions in an inverter's voltage and current signals. Thus, the most commonly used signal-based techniques for OCF diagnosis methods can be categorized into voltage-based [4, 5] and current-based [6, 7] approaches. In this regard, an OCF diagnosis method based on the stator current analysis is presented in [8]. Current-based approaches using the current space vector trajectory diameter and Park's vector method have been proposed in [9, 10]. However, these schemes are not preferred due to their associated disadvantages related to tuning and complexity. In addition, a two-line voltage attributes-based OCF diagnostic approach is presented in [11], which localizes an OCF in *l*/20 of fundamental period. In [12], a model-based approach with a line-to-line output voltage scheme is presented, where the preprocessed diagnosis eigenvalues are compared with a voltage envelope for a single switch OCF DaL. Current-based techniques require a relatively extended diagnostic duration (normally one fundamental period (FP)) to ensure higher OCF detection accuracy. However, voltage-based techniques have a lower fault diagnosis time and higher accuracy compared to current-based approaches. The key benefit of the current-based approach is its independence from system parameters with no additional hardware requirements. However, voltage-based techniques require extra voltage sensors, increasing the overall system cost, complexity, and potential fault vulnerability points. Moreover, adding additional sensors to a system affects the overall system topology as well, which is also not appreciated by the manufacturers. In addition, model-based techniques are also widely applied for fault diagnosis in motor drives. This method uses a variety of observers, such as sliding mode observer [13], variable structure observer [14], Luenberger observer [15], and nonlinear observer [16], which provides a relatively short diagnosis time with no additional hardware requirements. However, these methods are not preferred due to their performance being heavily dependent on the accuracy of the explicit system model and sensitivity to motor parameter deviations. On the other hand, data-driven approaches are based on the system's historical data [17] and can be applied to time-varying and complex nonlinear systems for OCF diagnosis without relying on machine models, trigger thresholds and load characteristics. Moreover, compared to the sturdy algorithms of signal-based and model-based methods, ML models are very versatile and can be easily extended to multiple fault diagnosis algorithms.

So, an ML approach with no need for an accurate system model or additional hardware and fast OCF detection can be a promising fault diagnosis technique to overcome some of the shortcomings of previously mentioned schemes. In this regard, various ML models based on random vector functional link (RVFL), convolution neural network (CNN), deep sparse filtering (DSF) network, deep belief networks (DBN) and least square support vector machine (LSSVM) have been proposed for OCF diagnosis [18, 19, 20, 21, 22]. Using more complex ML models may increase the detection accuracy but can also lead to computational burden and longer training time. This results in overrun problems during the practical implementation of an ML model. Therefore, an ML approach with a lower computation load and better accuracy is always preferred. So, in this work, rather than focusing on a more complex ML model to achieve better classification accuracy, a new way of OCF feature extraction with adequate classification accuracy is proposed. Where the conduction losses of each MOSFET obtained via ATM-based MPC are used as viable OCF feature data. The presented work integrates the ATM-based MPC with an LSTM-based ML model for OCF DaL, where the former provides additional physics-informed features via conduction losses, i.e., the feature's rich data, for the latter to classify effectively. The proposed approach utilizes the control layer's already available signals, avoiding additional computational or hardware requirements. Moreover, the contribution of this work can also be summarized as follows,

1. The notion of OCF DaL is introduced for ATM-based MPC.
2. The impact of single switch OCF on the conduction losses of each MOSFET in a two-level three-phase inverter is analyzed.
3. The efficiency of an LSTM-based neural network for OCF DaL by considering conduction losses associated with each MOSFET as a new OCF feature extraction mechanism is presented.

The rest of this paper is structured as follows. The EV powertrain architecture and control design section presents a general structure of an EDS with an ATM-based MPC mathematical model. The methodology section explains the neural network structure and the preferred datasets to be used for OCF diagnosis. Lastly, the experimental analysis and performance evaluation section illustrates the impact analysis of an OCF and the accuracy quantification of the proposed ML approach.

EV Powertrain Architecture and Control Design

A typical architecture of a modern EV system can be categorized into cyber (energy management system (EMS), controller, etc.) and physical system (traction inverter, interior permanent magnet synchronous motor (IPMSM), etc.). IPMSMs are widely used in EVs as traction motors because of their better efficiency, smooth torque output, and high power density. Each IPMSM is connected to a controller via a traction inverter while constituting a cyber-physical system.

ATM-Based Motor Drive Control Design

There are various control typologies for IPMSM motor drives. However, MPC is preferred due to its multi-objective, multi-constraint control features, reduced torque ripples, and better steady-state performance, along with an intuitive and coherent design approach [23, 24]. In addition, MPC can also be configured with active thermal control by coupling the electrical and thermal attributes of power converters, which is denoted as ATM-based MPC [25, 26, 27]. This enables the MPC to consider the thermal aspects of switching devices (SiC-MOSFETs) of power electronics converters in a multi-objective optimization problem that reduces the negative impacts of thermal cycling and thermal stress on power quality. Moreover, this thermal management approach also reduces the degradation and fault occurrence rate of MOSFETs by considering their junction temperature in terms of conduction and switching loss to obtain the optimal switching state. Therefore, ATM-based MPC can be considered a promising control approach for motor drive control design in automotive applications. The detailed schematic of the ATM-based MPC model for the IPMSM motor drive is shown in Fig. 1 with both physical

FIGURE 1 The Cyber-physical system of Motor Drive based on ATM-based MPC.

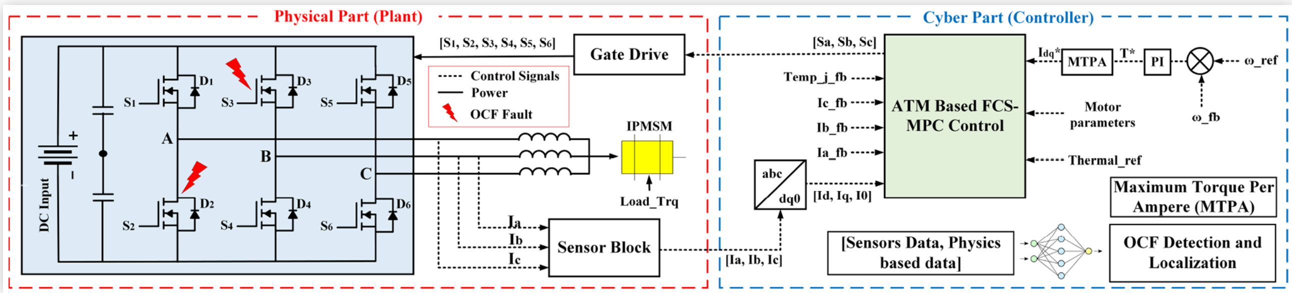

and cyber layers. The predicted values of current for IPMSM, based on model predictive current control (MPCC), can be obtained by using the forward Euler discretization approach as follows,

$$I^{p}_{d[k+1]} = \frac{L_d - t_{sc}R_s}{L_d} I_{d[k]} + \frac{t_{sc}L_qP}{L_d}\omega_{m[k]}I_{q[k]} + \frac{t_{sc}}{L_d}V_{d[k]} \quad (1)$$

$$I^{p}_{q[k+1]} = \frac{L_q - t_{sc}R_s}{L_q} I_{q[k]} + \frac{t_{sc}L_dP}{L_q}\omega_{m[k]}I_{d[k]} + \frac{t_{sc}}{L_q}V_{q[k]} - \frac{t_{sc}\psi_f P}{L_q}\omega_{m[k]} \quad (2)$$

Where I_d, I_q, V_d, V_q, L_d, and L_q are the winding current, voltage, and inductance of IPMSM in the dq frame of reference, respectively. In addition, R_s is the average winding resistance per phase, t_{sc} is the control layer sampling rate, P is the number of poles, ψ_f is the permanentmagnet flux linkage, and ω_m is the mechanical speed of IPMSM.

Power Loss Modelling

The most prominent losses in power electronics converters are conduction and switching loss of semiconductor switching devices. These power losses are calculated by using the predicted dq-axis currents from (1) and (2), along with the associated characteristics obtained from the manufacturer's datasheet. The pattern of current conduction for each power switch and diode of phase A for different switching states of S_1 and S_2 at positive and negative phase currents are described in Table 1. This table concludes that the positive current (current flowing outward from the inverter) can either flow through the upper power switch or lower diode, and the negative current (current flowing inward to the inverter) can only flow through the lower power switch or upper diode for each phase. This specific sequence is due to the defined placement and connectivity of these semiconductor devices. Moreover, the on and off-state currents for each switching state of MOSFET in Table 1 can be obtained via predicted current values for each phase. The conduction losses for the MOSFET and diode can be formulated as given in (3a) and (3b), respectively.

$$P^{mft}_{cond} = I^{2}_{ds} {}^{*}R_{ds(on)} \quad (3a)$$

$$P^{d}_{cond} = I_F {}^{*}V_F \quad (3b)$$

FIGURE 2 The steps for the proposed ML method for OCF DaL

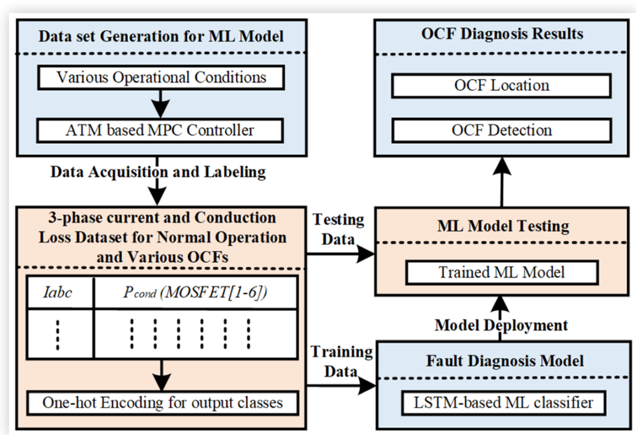

TABLE 1 Current Conduction Sequence for MOSFETs and Diodes in Phase-A under various operating conditions

S_1 State	S_2 State	Current Direction	Conduction pattern (Phase-A) S_1	S_2	D_1	D_2
ON	OFF	$i_a > 0$	Yes	No	No	No
ON	OFF	$i_a < 0$	No	No	Yes	No
OFF	ON	$i_a > 0$	No	No	No	Yes
OFF	ON	$i_a < 0$	No	Yes	No	No
OFF	OFF	$i_a > 0$	No	No	No	Yes
OFF	OFF	$i_a < 0$	No	No	Yes	No

$$P_{cond}^{total} = P_{cond}^{mft} + P_{cond}^{d} \tag{3c}$$

Where I_{ds} is drain-to-source current, and $R_{ds(on)}$ is a varying on-state resistance for MOSFET based on the I_{ds} and junction temperature. For (3b), I_F is the current for the anti-parallel diode, and V_F is the voltage drop across the diode under forward-bias condition. The total power loss for each of the semiconductor devices per sampling period can be calculated by using (3c). The characteristics obtained from the datasheet of the SiC half-bridge module with model number Cree/Wolfspeed CAB530M12BM3 (1200V, 530A) are used for the power loss modeling in this proposed study. In addition, for the sake of simplicity in terms of OCF DaL, only conduction losses are considered in the power loss modeling of the ATM-based finite control set (FCS) MPC model. Moreover, based on the similarities between electrical and thermal dynamics, a lumped parameter thermal network (LPTN) is used to analytically model the thermal states of semiconductor devices as given in [25, 28].

Cost Function

A multi-objective linear cost function is formulated based on the dq axis currents and thermal control of semiconductor devices.

$$J_{elec} = \left| I_d^{ref} - I^p_{d[k+1]} \right| + \left| I_q^{ref} - I^p_{q[k+1]} \right| \tag{4a}$$

$$J_{th} = \sum_{i=1}^{N} \left| T^{ref}_{j(i)} - T^{[k+1]}_{j(i)} \right| \tag{4b}$$

$$J_{total} = \min\left(\omega_e J_{elec} + \omega_t J_{th} \right) \tag{4c}$$

Where J_{elec} and J_{th} control the electrical and thermal performance of the traction inverter. I_d^{ref} and I_q^{ref} are reference values for the complex current components. Similarly, $T^{ref}_{j(i)}$ is the reference junction temperature for the i_{th} switch with N as the total number of switches and $T^{[k+1]}_{j(i)}$ is the associated predicted junction temperate for the i_{th} switch obtained as given in [25]. The objective is to minimize the multi-objective cost function (4c) with respect to reference values. In addition, ω_e and ω_t are the weighting coefficients that can control the performance of the power electronics converter as $\omega_e + \omega_t = 1$.

FIGURE 3 LSTM-based neural network for OCF DaL

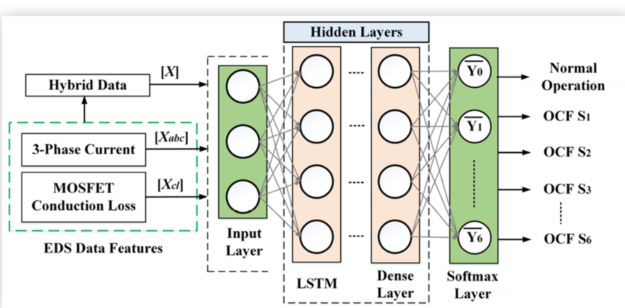

Methodology

The structure of the proposed ML approach leveraging conduction losses as a salient feature for OCF diagnosis in a three-phase inverter is shown in Fig. 2. Initially, a dataset including 3-phase current and conduction losses of each MOSFET is generated for the motor drive system shown in Fig. 1 under various operating conditions. This dataset is assigned distinct labels for each system state using one-hot encoding. Then, the data is split into training and testing datasets, with 70% of the data used for training and the remaining 30% for testing. The operational reliability of a model-free ML approach is very much based on the garbage-in garbage-out (GIGO) concept. Therefore, a non-redundant, balanced, and clean training dataset having a better correlation with output classes will result in better predictions. Finally, an LSTM-based ML classifier is trained and tested for OCF DaL in this study. LSTM is preferred due to its various advantages, such as insusceptibility to vanishing gradient problems and the capability to better capture the temporal patterns of time series data with long-term data dependence capabilities. This LSTM-based neural network is incorporated with the physics-based prior system information in terms of conduction losses of each MOSFET to further enhance the ML model's learning capabilities, defined as physics-informed machine learning (PIML) [29].

The Critical EDS Features and Neural Network

An optimized neural network model utilizing certain physics-based characteristics associated with each type of disturbance can effectively distinguish between various output classes. All physical faults produce a specific regular impact on system response due to their rooted physical model. Similarly, OCFs also have a particular influence on various system variables. In particular, Fig. 4 shows the disruption in the flow of currents in each phase due to the OCF in phase A. Moreover, when an OCF occurs in a MOSFET, it will no longer be able to conduct the current, resulting in zero conduction losses. In this regard, most past studies consider the phase currents I_a, I_b, and I_c as the most implicit parameters for the power transistor's fault analysis. However, by using the inherent property of ATM-based MPC, these three-phase currents can be decoupled for each of the MOSFET modules, which in return estimates the conduction losses via (3) for every switching sample, as shown in Fig. 7. These conduction losses can be used as an effective physics-based data feature to locate the OCF fault for MOSFETs within the traction inverter. So, the

X_{cl} vector, representing the MOSFETs conduction losses, correlated with output class labels, can be expressed as follows,

$$\mathbf{X_{cl}} = \left[P^{Loss}_{mft(i)}, P^{Loss}_{mft(i+1)}, \dots, P^{Loss}_{mft(i+5)}\right] \quad (5)$$

$$\mathbf{X_{abc}} = \left[I_a, I_b, I_c\right] \quad (6)$$

$$\mathbf{X} = \left[\mathbf{X_{cl}}, \mathbf{X_{abc}}\right] \quad (7)$$

where $P^{Loss}_{mft(i)}$ represents the total conduction losses of a MOSFET module, with i = 1. The structure of a MOSFET module consists of a MOSFET and an anti-parallel diode. Hence, $P^{Loss}_{mft(i)}$ indicates the sum of conduction losses associated with both of these components. In addition, X_{abc} represents the dataset with measured three-phase output currents and X as the total dataset containing both 3-phase currents and conduction losses. The accuracy of the LSTM classifier is tested for all three datasets in (5), (6), and (7). During the normal and abnormal operation of the system, these losses are periodic in nature, with a half-cycle associated with MOSFET and the other half-cycle to diode. The peak and frequency of these loss values will change based on the reference input of EDS. As a result of an OCF, the losses of MOSFET turn to zero, whereas the linked diode still conducts and reflects an increase in conduction losses due to an increase in current, as shown in Fig. 4 and 5. So, the MOSFET module with increased conduction loss of diode and zero losses for the MOSFET switch is used by the LSTM-based classifier as an implication to localize the OCF for each MOSFET. In this work, the case of single-switch OCF is considered; therefore, there are a total of seven output classes for LSTM classifier $Y_0 ... Y_6$, as shown in Fig. 3. The hidden layer consists of LSTM and dense layers. The output layer with softmax activation function transforms the predicted values into a probability distribution for all output classes, with the total sum equal to 1. The softmax function can be defined as,

FIGURE 4 Disturbances in the 3-phase current of power converter due to OCF. (a) OCF in MOSFET-1, (b) OCF in MOSFET-2 (Phase-A, Phase-B, Phase-C)

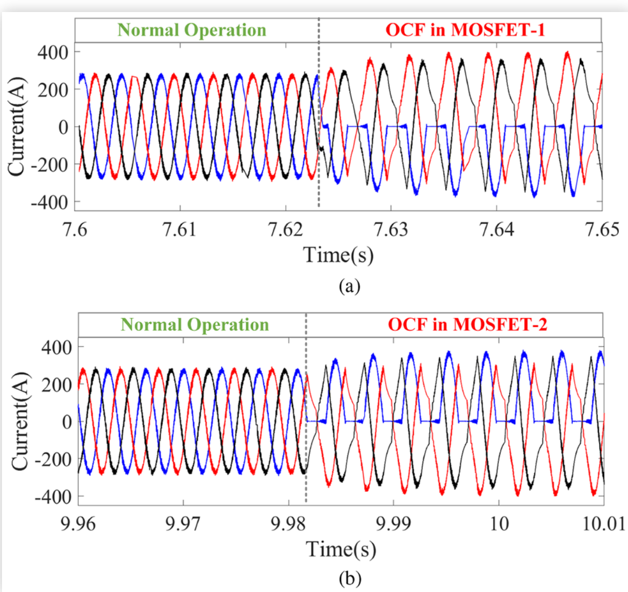

FIGURE 5 Conduction loss in MOSFET-1 and MOSFET-2 during normal operation and OCF. (a) OCF in MOSFET-1, (b) OCF in MOSFET-2

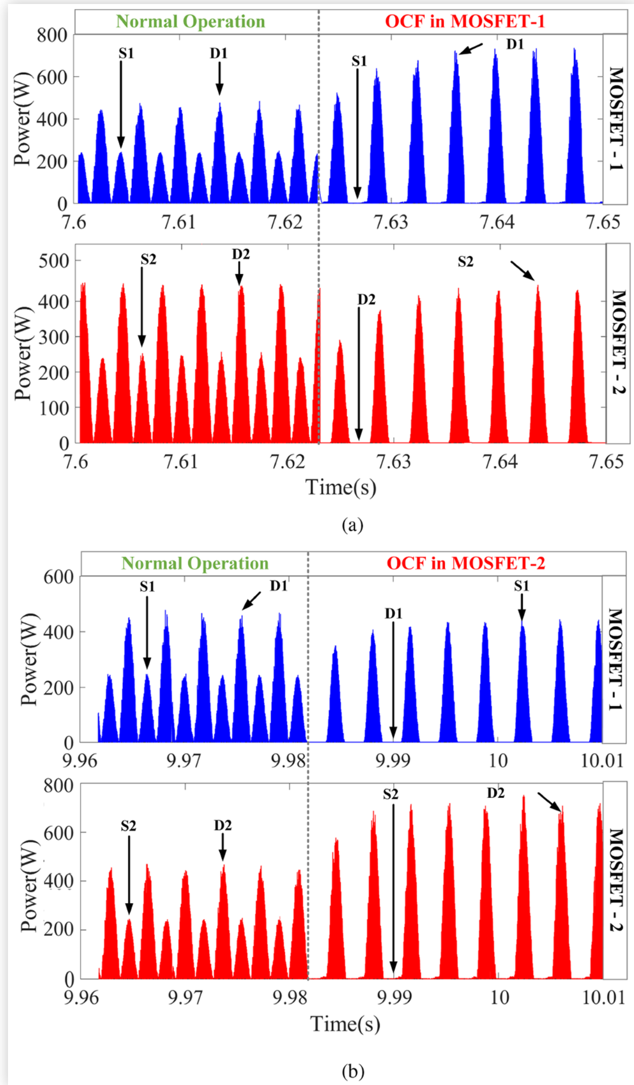

$$\text{Softmax}(\vec{x})_i = \hat{y}_j = \frac{e^{x_i}}{\sum_{j=1}^{n_c} e^{x_j}} \quad (8)$$

Where x_i represents the factors of the predicted vector from the dense layer, and n_c is the sum of all target classes. These target classes are obtained during data pre-processing via one-hot encoding. Finally, to minimize the error between anticipated labels $(\hat{y}_j)$ and ground truth (y_j), a mean squared error-based cost function is used, which can be expressed as follows,

$$\min J_{(mse)} = \frac{1}{N}\sum_{j=1}^{n_c}\left(y_j - \hat{y}_j\right)^2 \tag{9}$$

Where N is the sum of total training data points. Moreover, the concept of a confusion matrix is used to estimate the different performance evaluation metrics, such as accuracy, precision, and recall, for the proposed LSTM-based classifier.

Simulation Analysis and Performance Evaluation

This section investigates the impact analysis of OCFs on device-level signals of power converter along with performance evaluation of the proposed ML classifier for OCF DaL. The EDS architecture shown in Fig. 1 is simulated in MATLAB Simulink platform with a sampling time of 25us. The EDS dynamics associated with conduction losses of each MOSFET are analyzed for various case study scenarios. Finally, to illustrate the validity of the presented work, the prospective approach is tested for two different datasets and hyperparameters.

OCF and Conduction Loss Analysis

The section discusses the impact of single switch open-circuit fault (SSOF) on the 3-phase output current and conduction losses associated with each semiconductor device in the power converter. The OCF condition is simulated by continuously considering the gate signal of a MOSFET as zero. In addition, for a 2-level 3-phase inverter, each upper and lower MOSFET for a single phase produces the output current's positive and negative half-cycles. Therefore, when an OCF occurs in a single switch, it clips the associated output half-cycle, as shown in Fig. 4. In addition, Fig. 4a shows the output current of the power converter for normal operation and SSOF condition in S_1. So, for this scenario, the positive half cycle for phase-A is clipped, as the positive current can no longer conduct through S_1 due to OCF. Similarly, when SSOF will occur in S_3 and S_5, the positive half cycles for phase-B and C will also be clipped. In addition, when OCF occurred in lower-MOSFET (S_2), the negative half-cycle of output current turned to zero continuously, as the negative current can no longer conduct through S_2, as shown in Fig. 4b. In addition, a similar effect will also reflect for phase-B and C currents when S_4 and S_6 are under OCF. Moreover, when an SSOF occurs in one phase, the impact on frequency, magnitude, and phase also propagates to the remaining phases as well, which can also be examined via a fast Fourier transform.

Fig 5 shows the variation in conduction losses of MOSFETs and antiparallel diodes in phase-A when OCF occurred in S_1 and S_2. In case I, as shown in Fig. 5a, during

FIGURE 6 Conduction loss in MOSFET-3, MOSFET-4, MOSFET-5, and MOSFET-6 during normal operation and under OCF in MOSFET-1.

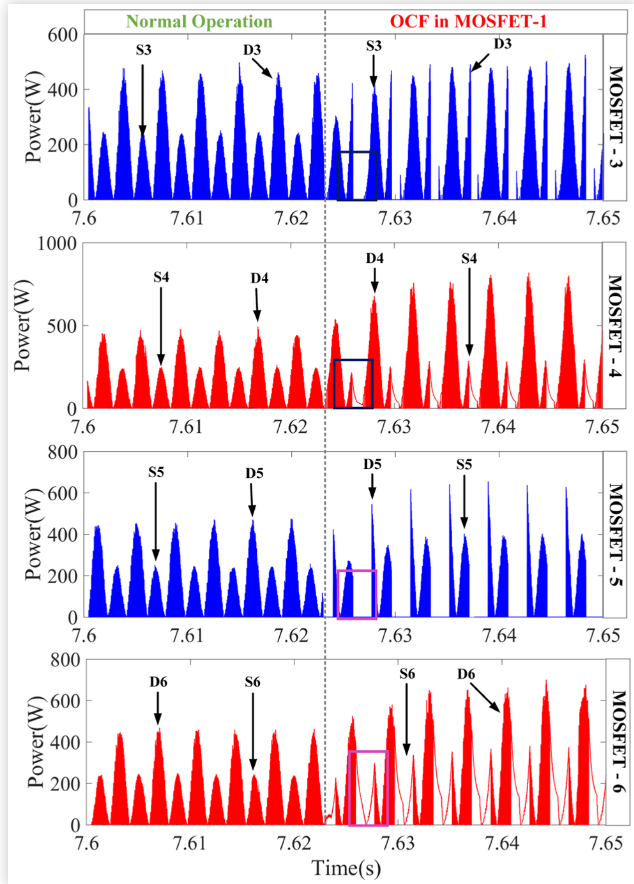

normal operation, the conduction losses exist consecutively for each MOSFET and diode, where the diode has a higher loss value with a peak of ≃400W and MOSFET illustrate lower losses with a peak value of ≃200W. These losses are calculated by applying the curve fitting technique on the characteristics curves in the datasheet of these semiconductor devices. The conduction losses remain the same in each half cycle for both MOSFETs and diodes of Phase-A during normal operation. Whereas, when OCF occurred in S_1, the conduction loss turns to zero for S_1 and D_2 because conduction of the positive current of phase-A is no longer possible due to OCF in S_1. Moreover, there is an increase in the conduction losses for D_1 and S_2 because of the increase in the peak of negative current, as shown in Fig. 4a. However, during the OCF in S_1, the overall losses for the upper MOSFET are more compared to the lower MOSFET because the diode is conducting for the upper MOSFET, which inherently has high conduction losses. In addition, when OCF occurred in S_2, the losses for D_1 and S_2 become zero, as the negative half current of phase A can no longer conduct, as shown in Fig. 5b. After an OCF in S_2, the upper MOSFET module has only MOSFET losses, and the lower module has diode losses with much higher values compared to MOSFET. Hence, it shows that the MOSFET module under OCF experiences higher conduction losses than other MOSFET modules in the same phase, which can also be used as a feature for fault DaL.

Furthermore, Fig. 6 shows the variations in conduction losses for the remaining MOSFET modules in phase-B and C when there was an OCF in S_1. It is evident that the variations in the conduction losses for the rest of the semiconductor switches have more fluctuations and are not similar to Fig. 5. Still, there are some instances where these losses are zero. During normal operation, a MOSFET or diode doesn't conduct continuously for each sampling period, whereas MOSFETs and diodes take turns one after the other for each switching cycle, as shown in Fig. 7. In this regard, when MOSFET is conducting, the losses for the diode are zero and vice versa. In Fig. 6, the instances when losses are turned to zero are because the MOSFET showed an irregular behavior of continuous conduction in the same instances. These irregularities in conduction losses when it completely becomes zero for phases B and C are also highlighted in Fig. 4. Finally, these distortions in losses for all six MOSFETs with distinct dynamics can be fed to train an ML classifier, which can be further used for OCF diagnosis.

Effectiveness of the Proposed Physics-Based Features for OCF Detection and Localization

This section presents the accuracy of the proposed LSTM-based classifier to detect and locate an OCF for different training datasets and hyperparameters. An ML classifier can be trained for various training data frames to classify future input values and the effectiveness of these training data frames, which ultimately decide the classifier's performance, depends on various factors, such as correlation with target labels, training data size, and the presence of outliers. Typically, a feature's rich data will have a higher training accuracy, which further reflects itself with better classifier efficiency for unseen future values. Therefore, in this section, the accuracy of the proposed classifier is compared and analyzed for OCF DaL under various operating parameters and training data frames. The data frame showing better training accuracy is considered a viable choice for an ML network used in DaL. In most recent model-based studies, the power converter's output current characteristics are used for OCF DaL because they can better reflect system dynamics under various operating conditions. However, in this proposed study, physics-based features originating from ATM-based control of the power converter are first utilized to anticipate the conduction losses for each MOSFET and then further used for OCF diagnosis using an ML classifier. In this regard, the performance of the LSTM classifier is evaluated for three different categories of the dataset, including three-phase currents (data-driven Approach), Conduction losses of MOSFETs (Physics-Informed Approach), and both three-phase currents and conduction losses (Hybrid Approach). In addition, two datasets for two different operating conditions are illustrated as X_1 and X_2. These datasets, reflecting the dynamic behavior of the system with respect to 3-phase current and conduction losses, are obtained as a .csv file while considering OCF for each MOSFETs. These input data frames are fed individually and combined for the training of the LSTM classifier while considering 200 Epoch. The LSTM neural network is trained and tested for X_1 and X_2, along with window size [10,30] and learning rate [5ms,1ms]. The accuracy of these datasets for different learning rates and window sizes is shown in Fig. 8 to validate the proposed approach of using conduction loss for OCF DaL. The final accuracy results associated with each dataset and precision and recall of each output class for X_2 data set are shown in Table 2 and 3, respectively. It is evident from Fig. 8 and Table 3 that the hybrid approach, where the ML network is trained by using physics-based features and three-phase currents, performs better than the standalone physics-informed or data-driven approach. Moreover, the comparison between the proposed approach and signal-based approaches is also shown in Table 4, where window size=10 is multiplied by the controller sampling rate to estimate the detection time of the proposed approach. However, the requirement of a large volume of historical data of the system under various operating conditions and the complexity of LSTM-based networks can also result in longer training time and slow computation of the input data to predict the system status regarding OCF detection. In addition, only the electrical characteristics of a motor drive are considered in this study for the training purpose of neural network, so that the proposed approach can also

FIGURE 7 Normal conduction operation of diode and MOSFET

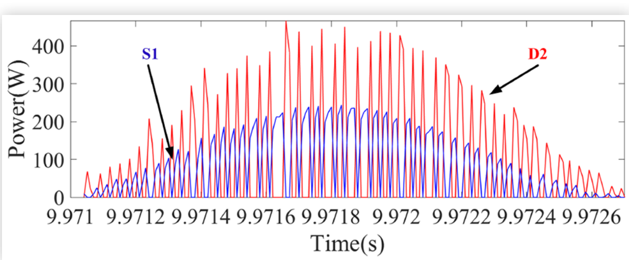

TABLE 2 OCF Detection Accuracy Results for two different data sets: [Training, Testing]%

	w_s = 10, Δt = 5ms			w_s = 30, Δt = 1ms		
Dataset Category	Data Driven	Physics-Informed	Hybrid approach	Data Driven	Physics-Informed	Hybrid approach
X_1	[80.97, 81.68]	[96.82, 96.91]	[98.81, 98.74]	[78.86, 79.03]	[97.68, 97.39]	[98.98, 98.81]
X_2	[79.01, 79.51]	[96.95, 96.34]	[99.08, 98.89]	[85.87, 85.80]	[97.92, 96.88]	[98.93, 99.01]

FIGURE 8 Accuracy curves of LSTM classifier for dataset X_1 and X_2

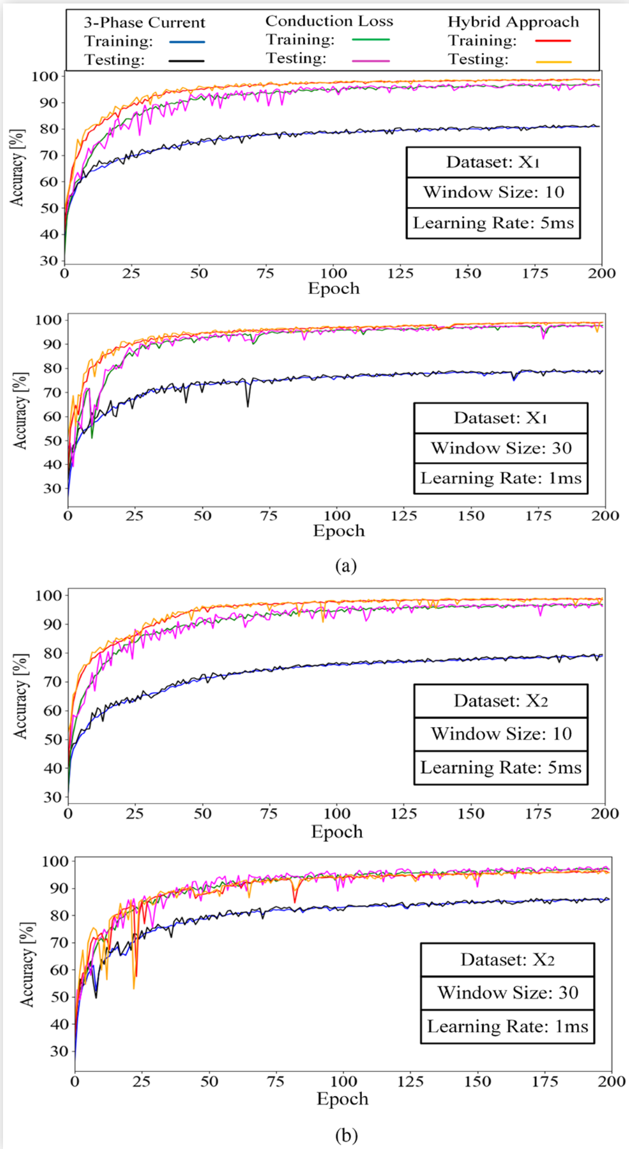

be considered viable for electrical power applications. Moreover, the conduction losses only require a 3-phase current as a main factor for its computation, so the proposed solution can also be used for conventional FCSMPC and FOC-centered controllers. In addition, the validity of the proposed approach can also be examined for particular scenarios associated with standard drive cycles such as US06 or WLTP2, which is the future target work of this proposed scheme.

Conclusion

This study provides an ML approach with unique and reliable feature rich data to detect and locate an OCF in a 2-level 3-phase inverter. The impact of OCF on the conduction losses of semiconductor devices and the performance of proposed ML approach is validated for various operating scenarios. The results shows that conduction losses obtained via ATM-based MPC approach can be used as a viable dataset for OCF DaL. Moreover, OCF localization is considered as first step for the development of a resilient control framework. Therefore, our future work will be based on the adaptive fault-tolerant control associated with OCF localization.

Acknowledgments

This work was supported by Clemson University's Virtual Prototyping of Autonomy Enabled Ground Systems (VIPR-GS), a US Army Center of Excellence for modeling and simulation of ground vehicles, under Cooperative Agreement W56HZV-21-2-0001 with the US Army DEVCOM Ground Vehicle Systems Center (GVSC). DISTRIBUTION STATEMENT A. Approved for public release; distribution is unlimited. (OPSEC 7987). The authors would like to express their gratitude for the valuable resources and facilities provided by the Secure Energy and Automation Laboratory (SEAL) and Real Time Controls and Optimization Laboratory (RTCOOL).

TABLE 3 Precision (P) and Recall (R) metrics for X_2, ω_s = 10, Δt = 5ms

	Data Driven		Physics Informed		Hybrid Approach	
Labels	**P**	**R**	**P**	**R**	**P**	**R**
Healthy(0)	0.97	1.00	1.00	1.00	1.00	1.00
OCF-1	0.78	0.79	0.91	0.98	0.98	0.99
OCF-2	0.79	0.78	0.98	0.96	0.99	0.98
OCF-3	0.76	0.79	0.97	0.93	0.99	0.98
OCF-4	0.79	0.74	0.95	0.95	0.98	0.98
OCF-5	0.77	0.74	0.98	0.96	0.99	0.99
OCF-6	0.75	0.76	0.96	0.98	0.99	0.99

TABLE 4 Performance Comparison between different OCF Diagnosis Methods

Methods	Detection Time	Accuracy	Implementation Cost
Current-based Methods	One FP	Good	No extra hardware required
Voltage-based Methods	<One FP	Good	High (needs extra voltage sensors)
Proposed ML Approach	0.25ms	Good	No extra hardware required

References

1. Timilsina, L., Badr, P.R., Hoang, P.H., Ozkan, G. et al., "Battery Degradation in Electric and Hybrid Electric Vehicles: A Survey Study," *IEEE Access* 11 (2023): 42431-42462.
2. Timilsina, L., Hoang, P.H., Moghassemi, A., Buraimoh, E. et al., "A Real-Time Prognostic-Based Control Framework for Hybrid Electric Vehicles," *IEEE Access* 11 (2023): 127589-127607.
3. Zhou, X., Sun, J., Li, H., Lu, M. et al., "Pmsm Open-Phase Fault-Tolerant Control Strategy Based on Four-Leg Inverter," *IEEE Transactions on Power Electronics* 35, no. 3 (2019): 2799-2808.
4. Zhou, D., Qiu, H., Yang, S., and Tang, Y., "Submodule Voltage Similarity-Based Open-Circuit Fault Diagnosis for Modular Multilevel Converters," *IEEE Transactions on Power Electronics* 34, no. 8 (2018): 8008-8016.
5. Zhou, D., Yang, S., and Tang, Y., "A Voltage-Based Open-Circuit Fault Detection and Isolation Approach for Modular Multilevel Converters with Model-Predictive Control," *IEEE Transactions on Power Electronics* 33, no. 11 (2018): 9866-9874.
6. Zhao, H. and Cheng, L., "Open-Switch Fault-Diagnostic Method for Back-to-Back Converters of a Doubly Fed Wind Power Generation System," *IEEE Transactions on Power Electronics* 33, no. 4 (2017): 3452-3461.
7. Gou, B., Ge, X.-L., Liu, Y.-C., and Feng, X.-Y., "Load-Current-Based Current Sensor Fault Diagnosis and Tolerant Control Scheme for Traction Inverters," *Electronics Letters* 52, no. 20 (2016): 1717-1719.
8. El Khil, S.K., Jlassi, I., Cardoso, A.J.M., Estima, J.O. et al., "Diagnosis of Open-Switch and Current Sensor Faults in Pmsm Drives through Stator Current Analysis," *IEEE Transactions on Industry Applications* 55, no. 6 (2019): 5925-5937.
9. Trabelsi, M., Boussak, M., and Gossa, M., "Multiple Igbts Open Circuit Faults Diagnosis in Voltage Source Inverter Fed Induction Motor Using Modified Slope Method," in:, *The XIX International Conference on Electrical Machines-ICEM 2010*, (IEEE, 2010), 1-6.
10. Freire, N.M., Estima, J.O., and Cardoso, A.J.M., "Open-Circuit Fault Diagnosis in Pmsg Drives for Wind Turbine Applications," *IEEE Transactions on Industrial Electronics* 60, no. 9 (2012): 3957-3967.
11. Wu, X., Chen, C.-Y., Chen, T.-F., Cheng, S. et al., "A Fast and Robust Diagnostic Method for Multiple Open-Circuit Faults of Voltage-Source Inverters through Line Voltage Magnitudes Analysis," *IEEE Transactions on Power Electronics* 35, no. 5 (2019): 5205-5220.
12. Shu, C., Ya-Ting, C., Tian-Jian, Y., and Xun, W., "A Novel Diagnostic Technique for Open-Circuited Faults of Inverters Based on Output Line-to-Line Voltage Model," *IEEE Transactions on Industrial Electronics* 63, no. 7 (2016): 4412-4421.
13. Shao, S., Wheeler, P.W., Clare, J.C., and Watson, A.J., "Fault Detection for Modular Multilevel Converters Based on Sliding Mode Observer," *IEEE Transactions on Power Electronics* 28, no. 11 (2013): 4867-4872.
14. Espinoza-Trejo, D.R., Campos-Delgado, D.U., Bossio, G., Bárcenas, E. et al., "Fault Diagnosis Scheme for Open-Circuit Faults in Field-Oriented Control Induction Motor Drives," *IET Power Electronics* 6, no. 5 (2013): 869-877.
15. Jlassi, I., Estima, J.O., El Khil, S.K., Bellaaj, N.M. et al., "Multiple Open-Circuit Faults Diagnosis in Back-to-Back Converters of Pmsg Drives for Wind Turbine Systems," *IEEE Transactions on Power Electronics* 30, no. 5 (2014): 2689-2702.
16. Campos-Delgado, D.U. and Espinoza-Trejo, D.R., "An Observer-Based Diagnosis Scheme for Single and Simultaneous Open-Switch Faults in Induction Motor Drives," *IEEE Transactions on Industrial Electronics* 58, no. 2 (2010): 671-679.
17. Timilsina, L., Hoang, P.H., Arsalan, A., Badr, B.R. et al., "Degradation Abatement in Hybrid Electric Vehicles Using Data-Driven Technique," *Transportation Research Procedia* 70 (2023): 52-60.
18. Gou, B., Xu, Y., Xia, Y., Deng, Q. et al., "An Online Data-Driven Method for Simultaneous Diagnosis of Igbt and Current Sensor Fault of Three-Phase Pwm Inverter in Induction Motor Drives," *IEEE Transactions on Power Electronics* 35, no. 12 (2020): 13281-13294.
19. Kim, S.-H., Yoo, D.-Y., An, S.-W., Park, Y.-S. et al., "Fault Detection Method Using a Convolution Neural Network for Hybrid Active Neutral-Point Clamped Inverters," *IEEE Access* 8 (2020): 140632-140642.
20. Liu, Z., Fang, L., Jiang, D., and Qu, R., "A Machine-Learning-Based Fault Diagnosis Method with Adaptive Secondary Sampling for Multiphase Drive Systems," *IEEE Transactions on Power Electronics* 37, no. 8 (2022): 8767-8772.
21. Shi, T., He, Y., Wang, T., and Li, B., "Open Switch Fault Diagnosis Method for Pwm Voltage Source Rectifier Based on Deep Learning Approach," *IEEE Access* 7 (2019): 66595-66608.
22. Arsalan, A., Timilsina, L., Papari, B., Muriithi, G. et al., "Cyber Attack Detection and Classification for Integrated on-Board Electric Vehicle Chargers Subject to Stochastic Charging Coordination," *Transportation Research Procedia* 70 (2023): 44-51.
23. Li, T., Sun, X., Lei, G., Yang, Z. et al., "Finite-Control-Set Model Predictive Control of Permanent Magnet Synchronous Motor Drive Systems—An Overview," *IEEE/CAA Journal of Automatica Sinica* (2022).
24. Poorfakhraei, A., Narimani, M., and Emadi, A., "A Review of Modulation and Control Techniques for Multilevel Inverters in Traction Applications," *IEEE Access* 9 (2021): 24187-24204.
25. Ozkan, G., Hoang, P.H., Badr, P.R., Edrington, C.S. et al., "Real-Time Thermal Management for Two-Level Active Rectifier with Finite Control Set Model Predictive Control," *International Journal of Electrical Power & Energy Systems* 131 (2021): 107057.
26. Moghassemi, A., Ozkan, G., Edrington, C.S., Muriithi, G. et al., "Active Thermal Control of Ac/Dc Power Converter Considering Health Monitoring of Power Modules," in:, *2023 IEEE Electric Ship Technologies Symposium (ESTS)*, (IEEE, 2023), 78-85.

27. Rahman, S., Ozkan, G., Arsalan, A., Chamarthi, P. et al., "Impact of Active Cooling on the Thermal Management of 3-Level NPC Converter for Hybrid Electric Vehicle Application," SAE Technical Paper 2023-01-1684 (2023), https://doi.org/10.4271/2023-01-1684.
28. Moghassemi, A., Rahman, S.I., Ozkan, G., Edrington, C.S. et al., "Power Converters Coolant: Past, Present, Future, and a Path toward Active Thermal Control in Electrified Ship Power Systems," *IEEE Access* (2023).
29. Xu, Y., Kohtz, S., Boakye, J., Gardoni, P. et al., "Physics-Informed Machine Learning for Reliability and Systems Safety Applications: State of the Art and Challenges," *Reliability Engineering & System Safety* 230 (2023): 108900.

ISSN 0148-7191